Available online at www.sciencedirect.com

ScienceDirect

Ceramics International 40 (2014) 2411–2417

CERAMICS INTERNATIONAL

www.elsevier.com/locate/ceramint

Electrochemical properties of Na_xCoO_2 ($x \sim 0.71$) cathode for rechargeable sodium-ion batteries

Alok Kumar Rai, Ly Tuan Anh, Jihyeon Gim, Vinod Mathew, Jaekook Kim*

Department of Materials Science and Engineering, Chonnam National University, 300 Yongbong-dong, Bukgu, Gwangju 500-757, Republic of Korea

Received 8 July 2013; received in revised form 31 July 2013; accepted 4 August 2013
Available online 20 August 2013

Abstract

In this work, almost pure Na_xCoO_2 ($x=0.71$) sample has been prepared via a solid-state route. The stoichiometric composition has been estimated by ICP-AES analysis and the Rietveld refinement performed on the respective XRD pattern led to an orthorhombic structure in the *Cmcm* space group with $a=2.83218(3)$ Å, $b=4.89983(4)$ Å, and $c=10.92334(14)$ Å. The insertion/deinsertion of sodium into the well-crystallized particles leads to capacities as high as 70.4 $mAhg^{-1}$ with an initial Coulombic efficiency of 90%, and excellent capacity retention of almost ~100% after the 90th cycle between a 2.0 and 3.5 V voltage window for a 0.08 C–rate. The insertion ratio (x) varied between 0.592 and 0.673 during the deinsertion/insertion process within Na_xCoO_2. The voltage profile shows numerous voltage steps being mainly associated to the slight ordering of the Na ions within the layers. By coupling the electrochemical process with an *in-situ* X-ray diffraction experiment, the *c-axis* and *a-axis* peak positions such as (002), (004) and (100) are shifted with the accompanying deintercalation/intercalation of sodium, suggesting that the extracted sodium has been reversibly occupied with a small variation in sodium composition ranges due to peculiar Na^+/vacancy ordering.

Keywords: A. Powders: solid state reaction; B. X-ray methods; E. Batteries

1. Introduction

Recently, the demands for lithium-ion batteries (LIBs) have been increasing due to their wide applications to power sources for cell phones, laptop computers, digital cameras, power tools and many consumer products; however, it is still a challenge to extend the applications of LIBs into electrical vehicles (EV) and hybrid electrical vehicles (HEV) as they require higher energy density, higher rate capability and longer life cycles [1,2]. In this context, it is important to note that large scale batteries may become more popular for electric vehicles/energy storage devices in the next few years. Although widely distributed in the earth′s crust, lithium is not regarded as an abundant element. Also, the data ensures that the cost of lithium raw materials has increased since its first practical application in 1991, and it may drastically increase as the demand increases through commercialization of large-scale lithium-ion accumulators for automotive applications in the near future. It is therefore essential to explore new ion sources that can be used or satisfy expected future demands.

In contrast to lithium, sodium resources are unlimited, and sodium is the second-lightest and smallest alkali metal next to lithium. Additionally, sodium-ion batteries also have some attractive features such as good economic efficiency, lower materials costs, low toxicity, improved safety characteristics and the ability to utilize electrolytes of low decompositional potential [3]. On the other hand, the electrochemical equivalent and standard potential of sodium are the most advantageous for aprotic battery applications after lithium. In fact, recent research is aimed at exploring potential candidates as both negative and positive electrodes of sodium-ion batteries. Recently, some electrodes such as $Na_2Ti_6O_{13}$, $NaFePO_4$, $NaCoPO_4$, $NaTi_2(PO_4)_3$, $NaFeF_3$, and $NaCrO_2$ were shown to demonstrate reversible insertion/deinsertion of sodium ions in sodium-ion batteries [4–8].

Non-stoichiometric compounds that can reversibly incorporate foreign atoms in their lattice without any modification in the

*Corresponding author. Tel.: +82 62 530 1703; fax: +82 62 530 1699.
E-mail address: jaekook@chonnam.ac.kr (J. Kim).

0272-8842/$ - see front matter © 2013 Elsevier Ltd and Techna Group S.r.l. All rights reserved.
http://dx.doi.org/10.1016/j.ceramint.2013.08.013

local configuration of the host atoms or crystallographic structure remain significant for battery applications. In this context, layer-structured materials serve as promising hosts for guest-ions in solid-state batteries and hence layer-type dichalcogenides electrodes such as Na_xCoO_2, Li_xCoO_2 and $Li_{0.43}Na_{0.36}CoO_{1.96}$ have been investigated for sodium-ion batteries. More importantly, the system Na_xMO_2 (where M=Ti, V, Cr, Mn, Fe, Co, Ni), in which the alkali and transition metals have stronger tendencies to form layered structures due to the larger difference of ionic radii have been extensively studied [8–18]. Furthermore, several sodium compounds with mixed transition metals, having either tunnel or layered structures, such as $Na_xNi_{0.6}Co_{0.4}O_2$, $Na_xNi_yMn_{1-y}O_2$, have also been studied as positive electrode materials [19–23]. Therefore, it will be interesting to investigate the sodium insertion regarding these materials. From the above discussion, sodium batteries may offer significant merits but not yet still much worked out when compared with lithium. This may be due to the reason that the fascinating discovery of lithium ion batteries has suppressed this important area for many years.

Here, our main interest has been focused on layered sodium cobalt oxide ($NaCoO_2$). In this layered structure, the lattice is built up by sheets of edge-sharing CoO_6 octahedra between which the Na-ions are inserted with trigonal prismatic (P) or octahedral (O) coordination to oxygen atoms. More importantly, there are four distinctive structural forms of Na_xCoO_2 viz., α-, α'-, β- and γ- phases; they differ in the stacking sequence of the close-packed oxygen layers which are perpendicular to the *c-axis* [24]. The most prominent γ-phase (P2 type) permits sodium insertion within the composition range of $0.5 < x < 0.75$ and is characterized by a stacking sequence of close-packed oxygen atoms…ABBAABBA… with the oxygen atoms on each side of the Na layers being identical so that prismatic coordination is provided for the Na^+ ions. In addition, a study by Delmas et.al on different compositions of sodium cobalt oxides reveals that $Na_{0.7}CoO_{1.96}$ presents the largest theoretical energy density (260 $Whkg^{-1}$) when incorporated into electrochemical cells [11]. However, it is quite difficult to precisely determine the sodium content, and discrepancies remain in the literature for some reported superstructures.

In the light of the above discussion, the present study reports a systematic and detailed study on the synthesis, characterization and electrochemical performances of Na_xCoO_2 layered material for sodium-ion battery applications. Moreover, the sodium content plays the main role in the structure and clearly drives the system properties. To further confirm the exact sodium content, the structure of Na_xCoO_2 was verified by Rietveld refinement of the XRD pattern. In addition, we are providing a detailed structural characterization by X-ray diffraction (XRD), field-emission scanning electron microscopy (FE-SEM) and a complete electrochemical survey focused on the deinsertion/insertion mechanism of sodium in the Na_xCoO_2 structure. Moreover, *in-situ* diffraction studies of *c-axis* and *a-axis* were also carried out during the initial electrochemical deintercalation/intercalation to confirm the reversibility of sodium ion during electrochemical experiments.

2. Experimental

The material was prepared by a solid-state reaction with the stoichiometric amounts of sodium oxide (Na_2O, 80%, Aldrich) and cobalt oxide (Co_3O_4, 99.8%, Aldrich). The precursors (equivalent to metal ions) were intimately mixed and ball milled in acetone for 24 h at a rate of 100 rpm. The resulting mixture was washed by acetone before filtering using ceramic membrane funnels and vacuum drying at 120 °C for 12 h. The obtained sample was ground into a powder using a mortar and pestle and heated at 800 °C for 8 h with 5 °C/min in air atmosphere and followed by natural cooling. Due to unavoidable evaporation of some sodium at elevated temperatures, the final Na:Co ratio is always lower than that weighed out and may appear as a separate phase [25]. To obtain the accurate chemical composition of the product, chemical analysis of the synthesized materials was performed with an inductively coupled plasma atomic emission spectrometer (ICP-AES) on a Perkin-Elmer Optima 4300 DV model. To investigate further, the synchrotron X-ray powder diffraction data was collected at the 9B high resolution powder diffraction beamline of the Pohang Light Source. Data were collected over the angular 2θ range of 10–130.5° with a 0.01° step. The incident X-rays were monochromatized to the wavelength of 1.5476 Å by a double-bounce Si(111) monochromator. The detector arm of diffractometer had soller slits with an angular resolution of 2° a flat Ge{111} crystal analyzer, an anti-scatter baffle, and a scintillation detector. The particles morphology and size were observed by field emission-scanning electron microscopy (FE–SEM, S-4700 Hitachi). The electrochemical property of the Na_xCoO_2 sample was evaluated with sodium metal as the reference electrode. The charge/discharge properties of the sample were measured by assembling half cells in a glove box filled with Ar-gas. The working electrode was prepared by mixing active material (Na_xCoO_2), ketjen black (KB) and Teflonized Acethylene Black (TAB) in the weight ratio 7:3:5 respectively. The mixture was pressed onto a stainless steel mesh and vacuum dried at 120 °C for 12 h. A 2032 coin-type cell consisting of the cathode and sodium metal anode separated by a polymer membrane together with a glass fiber was fabricated in a glove box and kept for 12 h before the electrochemical measurements. The electrolyte employed was a 1 M solution of $NaClO_4$ dissolved in propylene carbonate (PC). The discharge/charge measurements (BTS-2004H, Nagano, Japan) were performed at room temperature over a potential range of 2.0–3.5 V vs. Na^+/Na at different current rates. Cyclic voltammetric measurement of the electrode was performed on an AUTOLAB potentiostat (PGSTAT302N) with a scan rate of 0.1 mV s^{-1} between 2.0 and 3.5 V (vs. Na^+/Na). The *in-situ* XRD measurements were conducted on 1D XRS KIST-PAL beam line from the Pohang Accelerator Laboratory (PAL) using a MAR345 image plate detector operating at 2.5 GeV with a maximum storage current of 200 mA. The X-ray beam was focused by a toroidal mirror and monochromatized to 12.4016 keV (0.9997 Å) by a double-bounce Si (111) monochromator. The double-bounce Si (111) monochromator and a Si (111) analyzer crystal were used to

provide a high-resolution configuration in reciprocal space. During the preparation of the *in-situ* cell, the electrode active material mixed with ketjen black and a TAB binder was cast on stainless steel mesh and assembled in a spectro-electrochemical cell. A loading of 7 mg active material was used. The cell was cycled to a fully charged/discharged state by a portable potentiostat at constant rate of 0.08 C in the voltage range 3.5–2.0 V. Kapton tape was applied on the apertures of the outer cases of the test cells. To focus on the *c* and *a* parameter evolution, only three 2θ narrow regions were defined (10–11°, 20.3–21.2°and 22.8–23.7°) to respectively follow the (002), (004) and (100) diffraction line displacements.

3. Results and discussion

A major drawback towards the use of Na_xCoO_2 for energy devices is the volatility of sodium at elevated temperatures. Recently, it has been suggested that the sodium-volatility may be somewhat exaggerated, and some of the sodium lost from the bulk phase may still be present within the sample [25]. To know the exact composition of sodium in Na_xCoO_2, the ICP-AES analysis was performed and the results indicate that the stoichiometric composition of the prepared sample corresponds to $Na_{0.74}CoO_2$. For further confirmation of sodium content, Rietveld refinement was performed using FULLPROF package [26] on the synchrotron XRD data of Na_xCoO_2. In the refinement, a pseudo-Voigt function and a linear interpolation between the set background points with refinable height were used to define the profile shape and the background, respectively. The occupancy parameters of the Co and O ions was fixed at their nominal composition while the occupancy parameter of the Na ion was varied (in order to estimate the exact composition), all other parameters, such as scale factor, zero correction, background, half-width parameters, the mixing parameters, lattice parameters, positional coordinates and thermal parameters, were varied in the course of refinement.

Structure refinement was first carried out using the well known hexagonal structure in the $P6_3/mmc$ space group [24,27,28]. This structural model however, could not account for the peak splitting in the higher 2θ region. For instance, the peak corresponding to the $2\theta \sim 66.3°$ appears to be doublet in the XRD pattern while it is indexed as a singlet in the structural model using $P6_3/mmc$ space group. A similar condition exists for other higher angle peaks. In order to account for these discrepancies we carried out Rietveld refinement using orthorhombic structure in the *Cmcm* space, as proposed by Zhou et al. [25]. The splitting nature of the peaks in the higher 2θ was completely accounted using this structural model. The content of Na ion was estimated to be 0.708(4) keeping the occupancy parameters of Co and O ions at its nominal compositions of 1 and 2, respectively, in the formula unit. Fig. 1 depicts the Rietveld fit between the observed and calculated profile for $Na_{0.71}CoO_2$ using the orthorhombic structure in the *Cmcm* space group. The impurity phase corresponding to monoclinic sodium carbonate

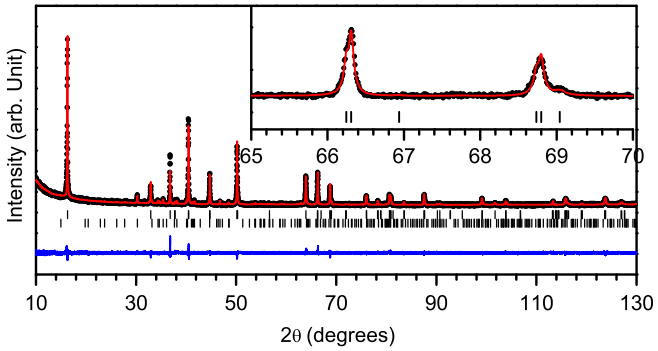

Fig. 1. Observed (black dots), calculated (red line) and difference (blue line) profiles obtained after full pattern Rietveld refinement using orthorhombic structure in the *Cmcm* space group for $Na_{0.71}CoO_2$. Bragg lines for the $Na_{0.71}CoO_2$ and Na_2CO_3 are also provided. Inset show the zoomed portions of the peaks in the 2θ range 65–70° showing the splitting nature (shown by two vertical tick marks at the bottom) of the peaks. (For interpretation of the references to color in this figure legend, the reader is referred to the web version of this article.)

(Na_2CO_3) belonging to the $C2/m$ space group in the XRD pattern was also taken into account during the Rietveld refinement. The vertical tick marks above the difference profile in the first and second lines from the top respectively, indicates the position of Bragg reflections for $Na_{0.71}CoO_2$ and Na_2CO_3 phases. A nearly flat difference profile indicates good quality of fitting between the observed and the calculated pattern. The refined structural parameters and *R* factors are summarized in Table 1.

The presence of Na_2CO_3 impurity may be due to the reaction between unreacted sodium and oxygen to form Na_2O. When exposed to air, Na_2O is easily converted to Na_2CO_3. It is highly possible that the presence of Na_2CO_3 impurity may be the reason for the difference in the Na content estimated from the ICP-AES (0.74) and the Rietveld refinement (0.71) analyses. The higher Na content calculated from the ICP-AES study may correspond to the overall sodium content since the Na present in the main and the impurity phases cannot be distinguished by ICP analysis. On the other hand, the Rietveld analysis considers the Na content specific to the main phase (Na_xCoO_2) and hence may yield comparatively lower sodium content than that estimated from ICP analysis. However, it may be reasonable to conclude that the stoichiometric composition obtained by the Rietveld analysis ($x=0.71$) is more dependable and hence the formation of $Na_{0.71}CoO_2$ in the present case may be realized according to the following chemical reaction:

$$3Na_2O + 2Co_3O_4 + 0.935O_2 \rightarrow 6Na_{0.71}CoO_2 + 0.87Na_2O\uparrow \quad (1)$$

Fig. 2 exhibits the FE-SEM image of $Na_{0.71}CoO_2$ after heat treatment at 800 °C for 8 h. The sample was composed of plate like crystals with a lateral dimension of micrometers and the plate-size is observed not to be uniform. From the FE-SEM image, it is clear that the average size of the $Na_{0.71}CoO_2$ plate is approximately of 2–5 μm diameters and 1 μm thick.

Table 1
Refined structural parameters of $Na_{0.71}CoO_2$.

Atom	Wyckoff site	*x/a*	*y/b*	*z/c*	*U* (Å^2)	Occ.
Co	4a	0.00000	0.00000	0.50000	0.0006(3)	1.0
Na1	8g	−0.083(6)	−0.019(3)	0.25000	0.019(4)	0.116(2)
Na2	8g	−0.057(6)	0.623(3)	0.25000	0.019(4)	0.238(2)
O	8f	0.00000	0.66667	0.5889(3)	0.0007(13)	1.0

$a=2.83218(3)$, $b=4.89983(4)$, $c=10.92334(14)$, $\alpha=\beta=\gamma=90^\circ$, space group *Cmcm*, $R_p=4.44$, $R_{wp}=5.78$, $R_{exp}=4.85$, $\chi^2=1.42$.

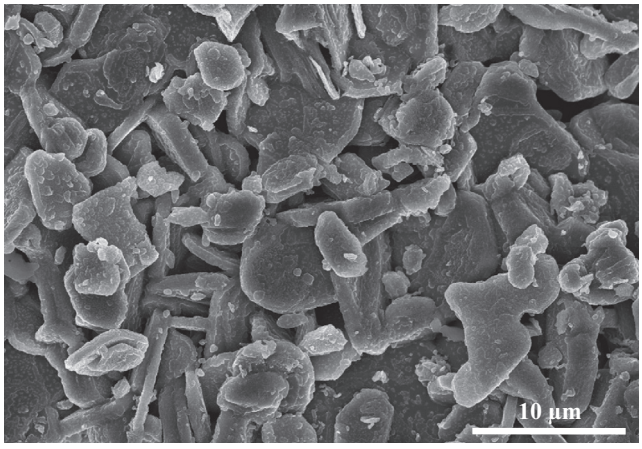

Fig. 2. FE-SEM micrograph of $Na_{0.71}CoO_2$ particles synthesized by solid-state reaction.

The result thus clearly indicates that it is difficult to obtain $Na_{0.71}CoO_2$ in nanometer scales with desired morphologies under the traditional high temperature solid-state method.

The electrochemical performance of $Na_{0.71}CoO_2$ was examined through galvanostatic charge/discharge cycling at 0.08 C in the potential range from 2.0 V to 3.5 V vs. the Na^+/Na reference electrode and the results are shown in Fig. 3. Fig. 3 (a) shows the charge/discharge voltage profiles of a $Na_{0.71}CoO_2$/Na cell at room temperature for the 1st, 2nd, 5th, 10th and 20th cycles. The almost consistent electrochemical behavior from the 2nd to the 20th cycle, plotted in Fig. 3(a), of the $Na_{0.71}CoO_2$ cathode indicates the stable cycle performance of the present electrode. Moreover, several short voltage plateaus attributed to various structural transitions in the crystal lattice of $Na_{0.71}CoO_2$ during electrochemical Na ion insertion and de-insertion are observed in the charge/discharge profiles. Recently, Delmas et al. published detailed studies on P2-Na_xCoO_2 in 2011, observing single-phase or two-phase domains during sodium ion intercalation/de-intercalation [27]. They suggested that, the existence of biphasic domains, characteristic of first-order transitions, on intercalation and deintercalation, leads to a voltage plateau. Potential drops are related to stable single-phase domains in a narrow sodium content range and the sloping curves are the signature of solid-solution behavior [27]. In the present case, irreversible capacity loss can be observed from the first charge/discharge profiles of the $Na_{0.71}CoO_2$ cathode. Approximately, 0.25 mol of Na, corresponding to an initial charge capacity of 63.1 mAhg^{-1}, can be deintercalated from $Na_{0.71}CoO_2$ when the cell is charged up to 3.5 V vs. Na/Na^+. Upon discharge to 2.0 V, ~0.28 mol of Na (corresponding to an initial discharge capacity of 69.7 mAhg^{-1}) can be reversibly intercalated back and the Coulombic efficiency corresponds to 90%. The charge curves at the first cycle are obviously different from the curves at the 2nd, 5th, 10th and 20th cycles, which are almost reversible without capacity fading. A reversible charge capacity of 75.2 mAhg^{-1} was achieved in the 2nd cycle, which is close to 74.1, 76.8, 76.8 and 76.1 mAhg^{-1} after the 5th, 10th, 15th and 20th cycles, respectively, whereas the Coulombic efficiency reached values higher than 83%.

Fig. 3(b) shows the charge/discharge capacity profile vs. the cycle number of the $Na_{0.71}CoO_2$ electrode at a rate of 0.08 C. It can be clearly observed that the present $Na_{0.71}CoO_2$ cathode showed long and stable cycle life under 0.08 C current rates. Most importantly, the capacity does not have a tendency to decline until the 90th cycle, which further indicates that Columbic efficiencies of almost 100% can be achieved on extended cycling. Precisely, after 90 cycles, specific capacities of approximately 70.4 mAhg^{-1} and almost 100% Coulombic efficiency was maintained by the $Na_{0.71}CoO_2$ cathode. The outstanding electrochemical performance of the present cathode makes it reliable application of sodium-ion battery applications. It is also reasonable to suggest that the excellent cycling performance of $Na_{0.71}CoO_2$ is possibly as a result of the formation of highly crystalline structures and suitable particle size, leading to a reversible phase transition.

Moreover, the C-rate behavior of $Na_{0.71}CoO_2$ cathode ranging from 0.008 C to 5.2 C is shown in Fig. 3(c). For each step, 3 cycles are measured in order to evaluate the capacity and capacity retention at different charge/discharge current conditions. The cell is first cycled at a low current rate of 0.008 C for 3 cycles, wherein stable average charge and discharge capacities of 91.5 mAhg^{-1} and 76.3 mAhg^{-1} are obtained, respectively. Furthermore, it can be seen that the discharge capacities are slightly reduced to 77.4, 73.8, 70.9, 68.7 and 62.3 mAhg^{-1} at rates of 0.02, 0.04, 0.08, 0.16, and 0.32 C, respectively. Even at a rate as high as 2.6 C, the electrode can deliver a discharge capacity of 28.8 mAhg^{-1}, which corresponds to a capacity retention of 38% compared to that obtained for the initial cycle. When the $Na_{0.71}CoO_2$ cell is operated at a high current rate, the capacity is decreased to an extremely low level. At the rate of 5.2 C, the capacity is only

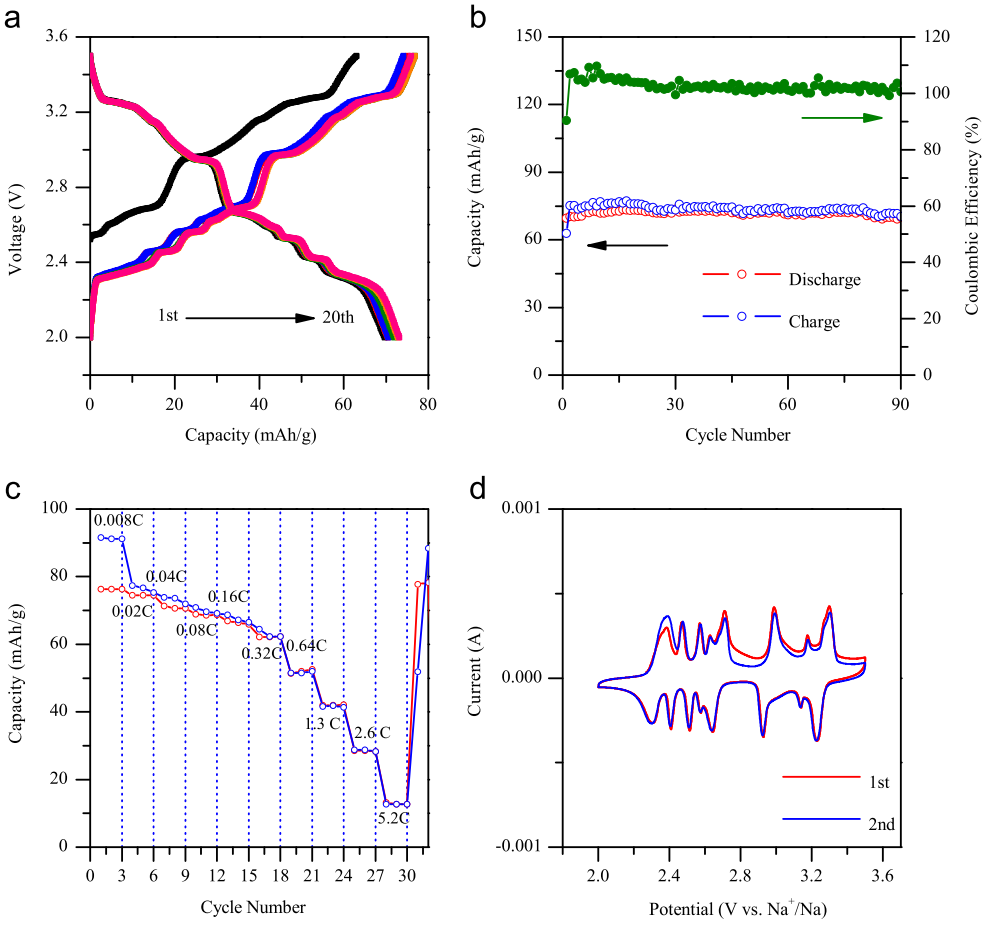

Fig. 3. Electrochemical performances of the $Na_{0.71}CoO_2$ electrode. (a) Charge/discharge voltage profiles between 2.0 and 3.5 V at the current rate of 0.08 C. (b) Capacity retention and coulombic efficiency plots under the current rate of 0.08 C. (c) The charge/discharge capacity at various C-rate is plotted. (d) Cyclic voltammograms at a scan rate of 0.1 mV s^{-1}.

12.7 mAhg^{-1}. The author believes that this is a result of the sluggish kinetics involved in the phase transition and the Na-ion diffusion in the solid state material, which can result in a significant loss of capacity at high current rates. In addition, when the testing current is regularly returned to a low current rate of 0.008 C, charge/discharge capacities comparable to that observed under similar current rate conditions during previous cycles are recovered.

The redox behavior of the present cathode is revealed further by the cyclic voltammograms (CV) curves. The CV curves of the first two cycles for the $Na_{0.71}CoO_2$ electrode are displayed in Fig. 3(d) in the voltage range of 2.0–3.5 V vs. Na^+/Na at a scanning rate of 0.1 mVs^{-1}. This can be seen from Fig. 3(d), whereby $Na_{0.71}CoO_2$ electrodes have eight pairs of oxidation and reduction peaks between low voltages to high voltages in the initial scan. It is reported that the initial irreversible phenomenon likely originates from the initial multi-atomic transition processes to accommodate the structural strain for Na ion insertion and extraction and from the surface reaction between the electrolyte and the electrode [29–30]. After the first scan, the second CV curves exhibit exactly the same number of redox peaks (eight) with the same intensities, shapes, and areas of the peaks, implying a complex multiphase transition mechanism during the Na-ion insertion and extraction processes [30]. However, *in-situ* XRD measurements, reported by Sauvage et al., suggested that it is difficult to distinguish the appearance of a new phase during Na ion insertion and extraction with only the shifts and splitting of a few peaks observed, indicating that the different structures during complex phase transitions are very closely related [30]. The observed result is also in good agreement with the reported galvanostatic cycling profiles and indicates a reversible and complex electrochemical reaction mechanism of the $Na_{0.71}CoO_2$ electrode vs. sodium.

To clearly evaluate the structural evolution of the entitled material during the insertion/de-insertion process, initial *in-situ* XRD measurements using specific cells comprising a stainless steel window as the current collector was undertaken and the results are shown in Fig. 4. Owing to the complex mechanism observed in the electrochemical profiles and the composition domains of the different phases involved, the in-situ measurement was performed at a rate of 0.08 C. In order to confirm the reaction mechanism, the evolution for the main intense *c-axis* and *a-axis* diffraction peaks such as (002), (004) and (100) respectively, which are very sensitive to the sodium content, was closely monitored. From the as-de-intercalated/intercalated materials of the initial charge/discharge between 3.5 and 2.0 V

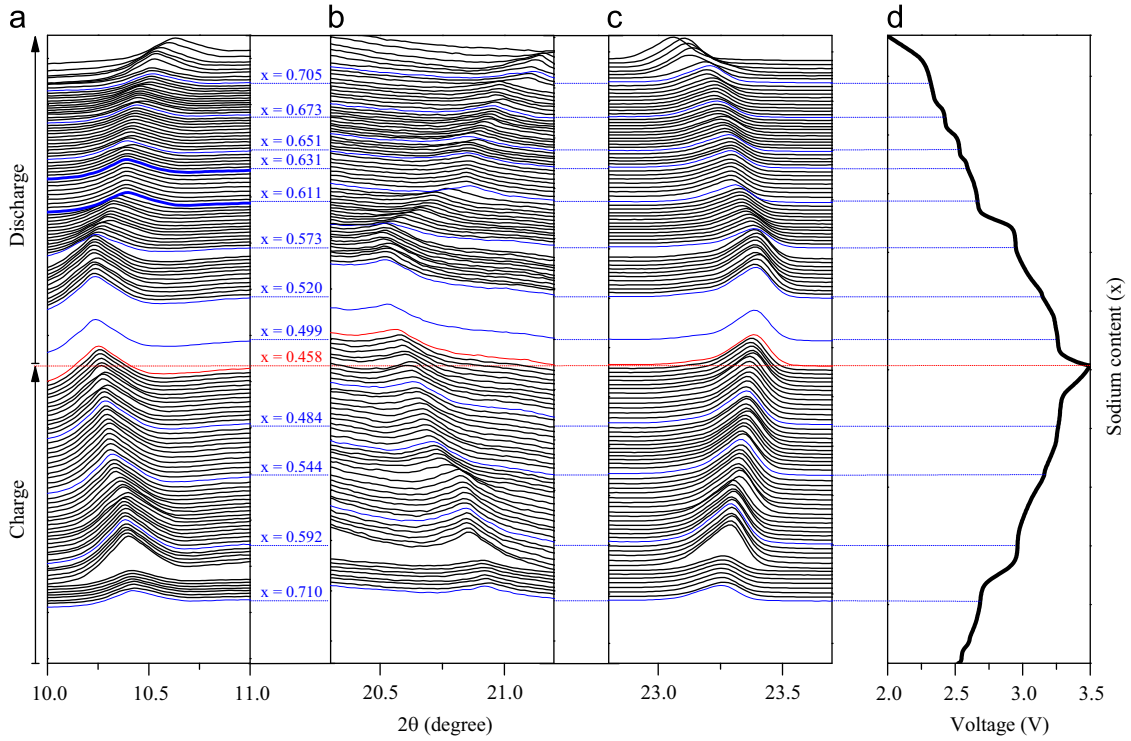

Fig. 4. *In-situ* evolution of the XRD pattern recorded at a 0.08 C during the initial charge/discharge of Na_xCoO_2 vs. Na cell (a) (002) diffraction, (b) (004) diffraction and (c) (100) diffraction peaks. Corresponding voltage-composition profile is given on the right side (d).

vs. Na^+/Na, clear shifts in the diffraction peaks corresponding to *c-axis* (002 and 004) toward lower and higher angles during charge and discharge, respectively, are observed. Whereas, the shifting trend is vice-versa for the diffraction peak corresponding to *a-axis*, i.e., the (100) diffraction peak shifts toward higher and lower angles during charge and discharge, respectively. This phenomenon is commonly observed in layered oxide materials [27,30]. It is worth mentioning here that during charge and discharge, the decrease and increase of the parameter is usually related to the oxidation and reduction of the transition metals in the metallic layer leading to a decrease and increase of their ionic radii, respectively. Moreover, the slight increase and decrease of the parameters is due to the removal and insertion of sodium in between the metallic layer, which decreases and increases the screening effect between the oxygen layers, respectively. As a result of the evolution of the XRD patterns in relation to the electrochemical curve, the formation of reversible sodium composition ranges ($0.673 < x < 0.710$) due to peculiar Na^+/vacancy ordering during de-insertion/insertion in Na_xCoO_2 and the closely-related structures are clearly demonstrated. It can be clearly observed that the existence of phases with obtained compositions is also reproducible. Further, it has also been reported that the observed sodium insertion domain $0.673 < x < 0.710$ displays a complex behavior with the formation of two consecutive adjacent biphasic domains not completely resolved at room temperature [27]. Moreover, the charge/discharge cycling curves exhibit potential plateaus, which are associated with (002), (004) and (100) diffraction peaks, as shown in Fig. 4(d). The slight shift in its 2θ position means that the single-phase domain adopts slight solid-solution behavior. On the contrary, a strictly fixed 2θ position during the potential drop proves the existence of a single phase with a well-defined composition [27].

4. Conclusions

In summary, a Na_xCoO_2 cathode was successfully synthesized by a solid-state reaction and was structurally characterized. The prepared sample was confirmed to the stoichiometry of $Na_{0.71}CoO_2$ by Rietveld refinement of the XRD pattern with orthorhombic symmetry (*Cmcm*, $a=2.83218(3)$ Å, $b=4.89983(4)$ Å, and $c=10.92334(14)$ Å) in addition to Na_2CO_3 impurity phases. The study clearly revealed that some sodium ions are lost from the bulk Na_xCoO_2 phase. A driving force for this is presumably associated with a reduction in the Na–Na repulsions, and this effect may only be prevalent in samples with high Na compositions. The results of galvanostatic testing showed specific capacities as high as 70.4 $mAhg^{-1}$ with an initial Coulombic efficiency of 90%, and an excellent capacity retention with ~100% Coulombic efficiency until the 90th cycle between a 2.0 and 3.5 V voltage window for a 0.08 C-rate. Cyclic voltammogram of the prepared $Na_{0.71}CoO_2$ showed eight couples of peaks in cathodic and anodic sweeps with close similarity to the voltages corresponding to the potential plateaus in the cycling profile of $Na_{0.71}CoO_2$. The cycling stability, reversibility, Coulombic efficiency, and rate capability make these Na-ion batteries attractive for possible low cost energy storage applications where modest energy density is required. By coupling the electrochemical process with an *in-situ* X-ray diffraction experiment, the *c-axis* and *a-axis* peak positions such as (002),

(004) and (100) are shifted with the accompanying deintercalation/intercalation of sodium, suggesting that the extracted sodium is reversibly occupied with a small variation in sodium composition ranges due to peculiar Na^+/vacancy ordering.

Acknowledgments

This research was supported by the Ministry of Science, ICT & Future Planning (MSIP), Korea, under the Convergence Information Technology Research Center (C-ITRC) support Program (NIPA-2013-H0301-13-1009) supervised by the National IT Industry Promotion Agency (NIPA). This work was also supported by the Basic Research Laboratories (BRL) Program No. (2009-0085441) of the National Research Foundation of Korea (NRF) funded by the Ministry of Science, ICT & Future Planning.

References

[1] J.M. Tarascon, M. Armand, Issues and challenges facing rechargeable lithium batteries, Nature 414 (2001) 359–367.
[2] P. Poizot, S. Laruelle, S. Grugeon, L. Dupont, J-M. Tarascon, Nano-sized transition-metal oxides as negative-electrode materials for lithium-ion batteries, Nature 407 (2000) 496–499.
[3] M. Armand, Oral presentation, in: Proceedings of the 16th International Meeting on Lithium Batteries, Montreal, Canada, June 2010.
[4] N.D. Trinch, O. Crosnier, S.B. Schougaard, T. Brousse, 5th International Lithium Battery Discussion Meeting, Arcachon, France, 12–17 June, 2011.
[5] R.A. Shakoor, Y.-U. Park, J. Kim, S.-W. Kim, D.-H. Seo, H. Gwon, K. Kang, Synthesis of $NaFePO_4$/$NaCoPO_4$ and their application to sodium batteries, Journal of the Korean Battery Society 3 (2010) 00.
[6] S.I. park, I. Gocheva, S. Okada, J. Yamaki, Electrochemical properties of $NaTi_2(PO_4)_3$ anode for rechargeable aqueous sodium-ion batteries, Journal of the Electrochemical Society 158 (2011) A1067–A1070.
[7] A. Kitajou, H. Komatsu, K. Chihara, I.D. Gocheva, S. Okada, Novel synthesis and electrochemical properties of perovskite-type $NaFeF_3$ for a sodium-ion battery, Journal of Power Sources 198 (2012) 389–392.
[8] S. Komaba, C. Takei, T. Nakayama, A. Ogata, N. Yabuuchi, Electrochemical intercalation activity of layered $NaCrO_2$ vs. $LiCrO_2$, Electrochemistry Communications 12 (2010) 355–358.
[9] E.J. Wu, P.D. Tepesch, G. Ceder, Size and charge effects on the structural stability of $LiMO_2$ (M=transition metal) compounds, Philosophical Magazine Part B 77 (1998) 1039–1047.
[10] T.A. Hewston, B.L. Chamberland, A Survey of first-row ternary oxides $LiMO_2$ (M=Sc–Cu), Journal of Physics and Chemistry of Solids 48 (1987) 97–108.
[11] C. Delmas, J.J. Braconnier, C. Fouassier, P. Hagenmuller, Electrochemical intercalation of sodium in Na_xCoO_2 bronzes, Solid State Ionics 3/4 (1981) 165–169.
[12] J.J. Braconnier, C. Delmas, P. Hagenmuller, Etude par desintercalation electrochimique des systemes Na_xCrO_2 et Na_xNiO_2, Materials Research Bulletin 17 (1982) 993–1000.
[13] A. Maazaz, C. Delmas, P. Hagenmuller, A Study of the Na_xTiO_2 system by electrochemical deintercalation, Journal of Inclusion Phenomena 1 (1983) 45–51.
[14] S. Kikkawa, S. Miyazaki, M. Koizumi, Electrochemical aspects of the deintercalation of layered AMO_2 compounds, Journal of Power Sources 14 (1985) 231–234.
[15] A. Mendiboure, C. Delmas, P. Hagenmuller, Electrochemical intercalation and deintercalation of Na_xMnO_2 bronzes, Journal of Solid State Chemistry 57 (1985) 323–331.
[16] L.W. Shacklette, T.R. Jow, L. Townsend, Rechargeable electrodes from sodium cobalt bronzes, Journal of Electrochemical Society 135 (1988) 2669–2674.
[17] Y. Takeda, K. Nakahara, M. Nishijima, N. Imanishi, O. Yamamoto, M. Takano, R. Kanno, Sodium deintercalation from sodium iron oxide, Materials Research Bulletin 29 (1994) 659–666.
[18] C. Didier, M. Guignard, C. Denage, O. Szajwaj, S. Ito, I. Saadoune, J. Darriet, C. Delmas, Electrochemical Na-deintercalation from $NaVO_2$, Electrochemical and Solid-State Letters 14 (5) (2011) A75–A78.
[19] I. Saadoune, A. Maazaz, M. Menetrier, C. Delmas, On the $NaxNi_{0.6}$-$Co_{0.4}O_2$ system: physical and electrochemical studies, Journal of Solid State Chemistry 122 (1996) 111–117.
[20] J.M. Paulsen, J.R. Dahn, Studies of the layered manganese bronzes, $Na_{2/3}[Mn_{1-x}M_x]O_2$ with M=Co, Ni, Li, and $Li_{2/3}[Mn_{1-x}M_x]O_2$ prepared by ion-exchange, Solid State Ionics 126 (1999) 3–24.
[21] Z. Lu, J.R. Dahn, In situ X-ray diffraction study of P2 $Na_{2/3}[Ni_{1/3}Mn_{2/3}]O_2$, Journal of Electrochemical Society 148 (2001) A1225–A1229.
[22] M.M. Doeff, T.J. Richardson, K.T. Hwang, Electrochemical and structural characterization of titanium-substituted manganese oxides based on $Na_{0.44}MnO_2$, Journal of Power Sources 135 (2004) 240–248.
[23] S. Komaba, T. Nakayama, A. Ogata, T. Shimizu, C. Takei, S. Takada, A. Hokura, I. Nakai, Electrochemically reversible sodium intercalation of layered $NaNi_{0.5}Mn_{0.5}O_2$ and $NaCrO_2$, ECS Transactions 16 (42) (2009) 43–55.
[24] K. Takada, H. Sakurai, E. Takayama–Muromachi, F. Izumi, R. A. Dilanian, T. Sasaki, Superconductivity in two-dimensional CoO_2 layers, Nature 422 (2003) 53–55.
[25] T. Zhou, D. Zhang, T.W. Button, A.J. Wright, C. Greaves, Influence of cooling rate on the structure and composition of Na_xCoO_2 ($x\sim0.65$), Journal of Materials Chemistry 19 (2009) 1123–1128.
[26] J. Rodriguez-Carvajal, FULLPROF, Laboratory Leon Brillouin CEA-CNRSCEA/Saclay, 91191 Gif sur Yvette Cedex, France, Version May 2010.
[27] R. Berthelot, D. Carlier, C. Delmas, Electrochemical investigation of the P2-Na_xCoO_2 phase diagram, Nature Materials 10 (2011) 74–80.
[28] R.J. Balsys, R.L. Davis, Refinement of the structure of $Na_{0.74}CoO_2$ using neutron powder diffraction, Solid State Ionics 93 (1996) 279–282.
[29] Y. Cao, L. Xiao, W. Wang, D. Choi, Z. Nie, J. Yu, L.V. Saraf, Z. Yang, J. Liu, Reversible sodium ion insertion in single crystalline manganese oxide nanowires with long cycle life, Advanced Materials 23 (2011) 3155–3160.
[30] F. Sauvage, L. Laffont, J.M. Tarascon, E. Baudrin, Study of the insertion/deinsertion mechanism of sodium into $Na_{0.44}MnO_2$, Inorganic Chemistry 46 (2007) 3289–3294.